PHYSICAL REVIEW ACCELERATORS AND BEAMS **20,** 104701 (2017)

Design of an X-band electron linear accelerator dedicated to decentralized ^{99}Mo/^{99m}Tc supply: From beam energy selection to yield estimation

Jaewoong Jang,[1,*] Masashi Yamamoto,[2] and Mitsuru Uesaka[1,3]

[1]*Department of Bioengineering, University of Tokyo, Bunkyo, Tokyo 113-8656, Japan*
[2]*Accuthera Incorporated, Kawasaki, Kanagawa 215-0033, Japan*
[3]*Nuclear Professional School, University of Tokyo, Naka, Ibaraki 319-1188, Japan*

(Received 21 February 2017; published 3 October 2017; corrected 18 October 2017)

The most frequently used radionuclide in diagnostic nuclear medicine, ^{99m}Tc, is generally obtained by the decay of its parent radionuclide, ^{99}Mo. Recently, concerns have been raised over shortages of ^{99}Mo/^{99m}Tc, owing to aging of the research reactors which have been supplying practically all of the global demand for ^{99}Mo in a centralized fashion. In an effort to prevent such ^{99}Mo/^{99m}Tc supply disruption and, furthermore, to ameliorate the underlying instability of the centralized ^{99}Mo/^{99m}Tc supply chain, we designed an X-band electron linear accelerator which can be distributed over multiple regions, whereby ^{99}Mo/^{99m}Tc can be supplied with improved accessibility. The electron beam energy was designed to be 35 MeV, at which an average beam power of 9.1 kW was calculated by the following beam dynamics analysis. Subsequent radioactivity modeling suggests that 11 of the designed electron linear accelerators can realize self-sufficiency of ^{99}Mo/^{99m}Tc in Japan.

DOI: 10.1103/PhysRevAccelBeams.20.104701

I. INTRODUCTION

Nuclear medicine is a branch of medical imaging where active ingredients labeled with medical radionuclides, called radiopharmaceuticals, are used for examining and treating diseases in a noninvasive way [1]. Each year, over 80% of nuclear medicine scans are performed with technetium-99m (^{99m}Tc) across the globe [2,3], attributed to its decay characteristics and chemistry ideal for radiopharmaceuticals.

Namely, ^{99m}Tc emits γ-rays of 140.5 keV, by which adequate spatial resolution can be obtained with a gamma camera optimized to that energy [2,4,5], and has a physical half-life of 6 hours, which leads to balanced effective half-lives of its radiopharmaceuticals and thereby allowing sufficient drug uptakes while limiting patient radiation doses [6,7]. Furthermore, ^{99m}Tc is able to form various radiopharmaceutical complexes, by virtue of its multiple oxidation states ranging from -1 to $+7$ [8–10].

In general, ^{99m}Tc is obtained through generation from the negatron (β^-) decay of molybdenum-99 (^{99}Mo), because the 11-fold longer physical half-life of ^{99}Mo can prolong the time during which ^{99m}Tc remains available [10,11]. In practice, ^{99}Mo having a high specific activity (HSA) is loaded on an alumina (Al_2O_3) column in a chromatographic device, referred to as a ^{99m}Tc generator, from which ^{99m}Tc is eluted with normal saline [12,13].

The majority of HSA ^{99}Mo is produced via the fission of uranium-235 (^{235}U) in research reactors [13,14] for a number of reasons: First, the ^{235}U fission cross section for thermal neutrons and the ^{99}Mo fission yield are as high as 584 b and 6.1%, respectively [3,13]. Second, several state-run multipurpose research reactors have been providing ^{235}U target irradiation services at near-cost prices using government subsidies [13,15]. Furthermore, weapons-grade highly enriched ^{235}U (HEU) which can greatly improve the ^{99}Mo productivity has been available to these reactors [3,13,14,16].

Currently, six such reactors are in operation around the world [13], shown in Fig. 1. All but one of them, however, are over 40 years old, facing component and system aging and thereby making the ^{99}Mo/^{99m}Tc supply chain subject to the associated interruptions. In 2009–2010, for instance, the National Research Universal (NRU) reactor in Canada and the High Flux Reactor (HFR) in the Netherlands concurrently shut down for component repairs, which brought about ^{99m}Tc shortages on a global scale [13,17]. Consequently, ^{99m}Tc-based medical procedures amounting to the shortfalls had to be canceled, postponed, or substituted with alternative ones [13,18].

Moreover, because of the end of service life, permanent shutdowns of the aging reactors in the near future are unavoidable: the OSIRIS reactor in France already shut down in December 2015 [13,19], and the NRU reactor will be decommissioned in March 2018 following its cessation of ^{99}Mo routine production in October 2016 [11,13].

---

[*] jang@nuclear.jp

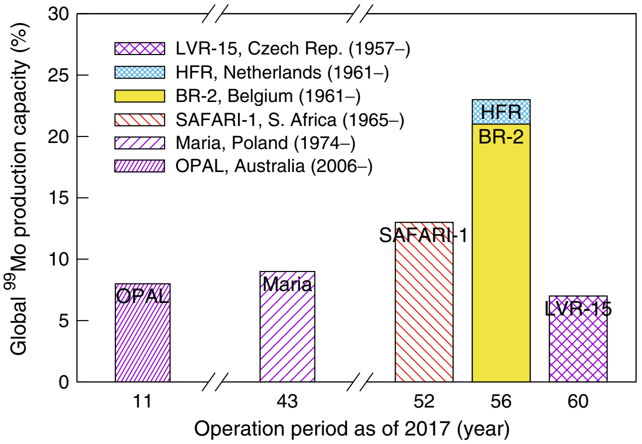

FIG. 1. Operation periods and global ^{99}Mo production capacities of large-scale research reactors.

On this account, several accelerator-based alternatives to the fission-based ^{99}Mo/^{99m}Tc production scheme have been explored, including (1) direct production of ^{99m}Tc via ^{100}Mo$(p,2n)^{99m}$Tc using a cyclotron [20,21]; (2) production of ^{99}Mo via ^{100}Mo$(n,2n)^{99}$Mo using a cyclotron as the neutron source [22]; and (3) production of ^{99}Mo via ^{100}Mo$(\gamma,n)^{99}$Mo using an electron linear accelerator (linac) as the photon source [7,23–30]. Among these proposals, we consider the electron-linac method a viable approach for the following reasons. (i) ^{99}Mo can be produced in large quantities by using the giant resonance of ^{100}Mo$(\gamma,n)^{99}$Mo [7,26,31]. (ii) Compared with the fission method, less diverse and less hazardous operational radioactive wastes are produced along with ^{99}Mo [3,11,26,32]. Also, ^{99}Mo production facilities can be decentralized by utilizing the smaller size of an electron linac, in which case the ^{99}Mo delivery time to end users can be reduced from around six days to one day. (iii) In contrast to the cyclotron-based ^{99m}Tc direct production [33–36], the interference in ^{99m}Tc radiopharmaceutical formulation by other Tc isotopes can easily be avoided by discarding a first ^{99m}Tc eluate from loaded ^{99}Mo.

We agree with the views presented by other authors [11,13,32] that the current global ^{99}Mo/^{99m}Tc supply chain is inherently fragile because the ^{99}Mo-producing reactor facilities are available only in a few specific countries. In this respect, we envision that producing ^{99}Mo over various regions by multiple electron-linac facilities can stabilize the ^{99}Mo/^{99m}Tc supply chain, for which we designed a dedicated compact *X*-band electron linac.

II. DESIGN OF *X*-BAND ELECTRON LINAC

A. Design considerations

If f denotes the operating frequency, the effective shunt impedance per unit length is proportional to $f^{1/2}$ in normal-conducting copper structures [37,38]. A higher radio frequency (rf) can therefore provide a higher accelerating gradient, which in turn offers structural compactness. Thus, we decided to use the 11.9942-GHz *X*-band rf [39] of the Compact Linear Collider (CLIC) [40], although many industrial and medical electron linacs operate at the subharmonic *S*-band rf [37,41,42].

A side-coupled biperiodic structure (SCS), which provides also a high shunt impedance despite its $\pi/2$-mode operation [38,43,44], was chosen to be the accelerating structure.

When setting the final electron beam energy, on the other hand, we made efforts such that the bremsstrahlung photons, generated at a naturally occurring tungsten ($^{\mathrm{nat}}$W) converter via $^{\mathrm{nat}}$W(e,γ), can have energies close to 14 MeV, the peak resonance energy of the ^{100}Mo photoneutron reaction ^{100}Mo$(\gamma,n)^{99}$Mo [45].

To make it clear, we outline the basic features of the linac as follows: (i) The final electron beam energy is 35 MeV, at which ^{99}Mo can be produced in sufficient quantities at reasonable capital costs. (ii) The first SCS is covered with a focusing coil to suppress its beam-breakup (BBU) instability [46]. (iii) Two accelerating modules are used, each composed of two SCSs and fed by one *X*-band 6 MW klystron.

The designed *X*-band electron linac is schematically illustrated in Fig. 2 [47].

B. Final electron beam energy

The strategy for setting the final electron beam energy was modeling and referring to the yield of photonuclear-produced ^{99}Mo. First, we modified a Bateman equation [48], such that it describes both the decay and production rates of ^{99}Mo radionuclides in a Mo target:

$$\frac{dN_p(t_{\mathrm{irr}})}{dt_{\mathrm{irr}}} = -\lambda_p N_p(t_{\mathrm{irr}}) + \mathcal{R}_{\mathrm{tar}}, \tag{1}$$

where N_p is the number of ^{99}Mo radionuclides, t_{irr} is the Mo target irradiation time, λ_p is the decay constant of ^{99}Mo, and $\mathcal{R}_{\mathrm{tar}}$ is the reaction rate of ^{100}Mo$(\gamma,n)^{99}$Mo over the Mo target volume $\mathcal{V}_{\mathrm{tar}}$, which we define as

$$\mathcal{R}_{\mathrm{tar}} \equiv \mathcal{V}_{\mathrm{tar}} \int_{E_{\gamma,\mathrm{min}}}^{E_{\gamma,\mathrm{max}}} \phi(E_\gamma)\Sigma(E_\gamma)dE_\gamma, \tag{2}$$

where ϕ is the time-independent bremsstrahlung flux in the Mo target, E_γ is the bremsstrahlung energy dependent largely on the electron beam energy E_e, and Σ is the macroscopic cross section of ^{100}Mo$(\gamma,n)^{99}$Mo.

Equation (2) is a consequence of

$$\phi(E_\gamma) = \frac{1}{\mathcal{V}_{\mathrm{tar}}} \iiint_{\mathcal{V}_{\mathrm{tar}}} \phi(\mathbf{r},E_\gamma)d\mathcal{V}_{\mathrm{tar}}, \tag{3}$$

with [49,50]

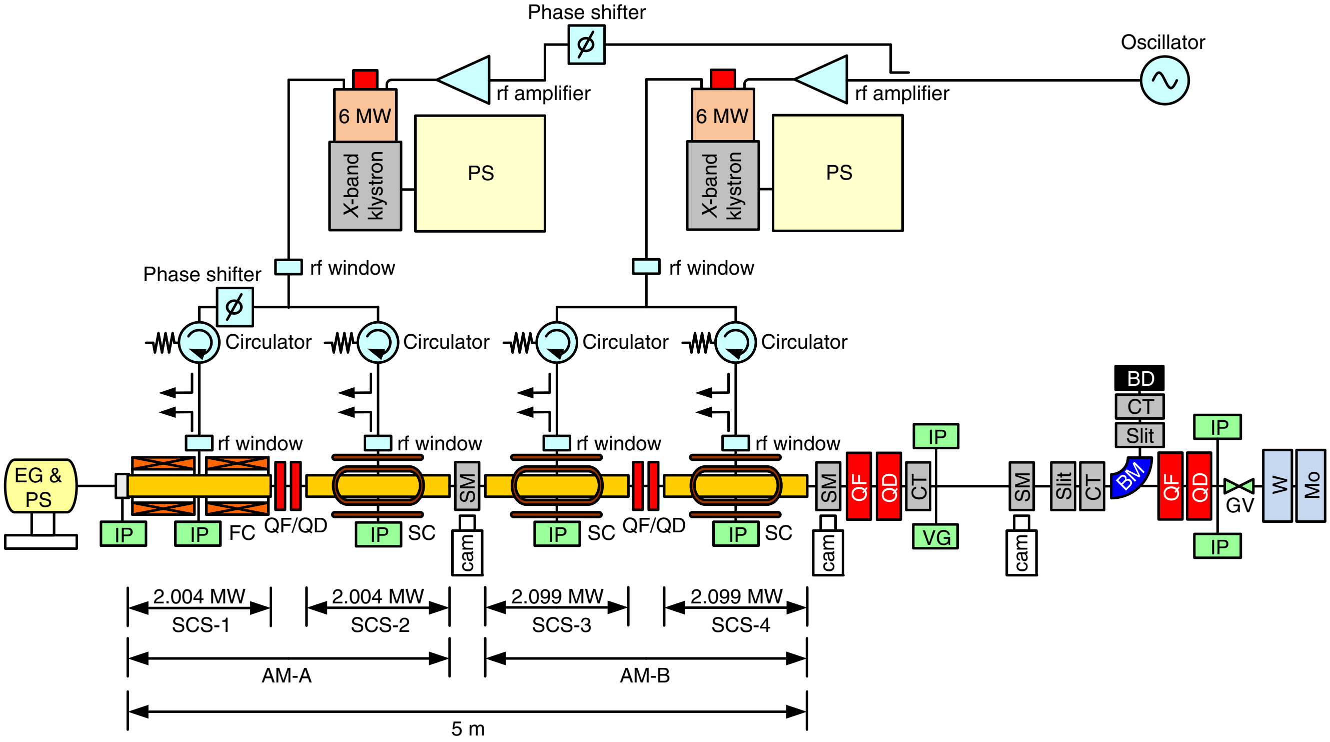

FIG. 2. Schematic representation of the *X*-band electron linear accelerator. The abbreviations are explained in Table I.

$$\phi(\mathbf{r}, E_\gamma) \equiv vn(\mathbf{r}, E_\gamma) = \frac{d\Phi(\mathbf{r}, E_\gamma)}{dt_{\mathrm{irr}}}, \tag{4}$$

where $\mathbf{r} \equiv x\hat{\mathbf{x}} + y\hat{\mathbf{y}} + z\hat{\mathbf{z}}$ is the position vector, and v, n, and Φ are the speed, number density, and fluence of the bremsstrahlung photons, respectively. The definition of ^{100}Mo$(\gamma, n)^{99}$Mo macroscopic cross section, on the other hand, is given by [49,50]

$$\Sigma(E_\gamma) \equiv \mathcal{N}_h \sigma(E_\gamma) = \left(\frac{\omega_h \rho}{M_h} N_A\right) \sigma(E_\gamma),$$

where $\mathcal{N}_h$ is the atomic number density of ^{100}Mo, σ is the microscopic cross section, ω_h is the mass fraction of ^{100}Mo, ρ is the mass density of the Mo target, M_h is the molar mass of ^{100}Mo, and N_A is the Avogadro constant.

TABLE I. List of abbreviations (Abbr) used in Fig. 2.

Abbr	Meaning	Abbr	Meaning
AM	Accelerating module	Mo	Molybdenum target
BD	Beam dump	PS	Power supply
BM	Bending magnet	QD	Defocusing Q-magnet
cam	Camera	QF	Focusing Q-magnet
CT	Current transformer	SC	Steering coil
EG	Electron gun	SCS	Side-coupled structure
FC	Focusing coil	SM	Screen monitor
GV	Gate valve	VG	Vacuum gauge
IP	Ion pump	W	Tungsten γ converter

Multiplying the solution of Eq. (1) by λ_p, we obtain the ^{99}Mo activity

$$A_p(t_{\mathrm{irr}}) = [1 - \exp(-\lambda_p t_{\mathrm{irr}})] \times \mathcal{V}_{\mathrm{tar}} I_b \int_{E_{\gamma,\mathrm{min}}}^{E_{\gamma,\mathrm{max}}} \Phi_{\mathrm{MC}}(E_\gamma) \Sigma(E_\gamma) dE_\gamma, \tag{5}$$

where I_b is the electron beam current, and Φ_{MC} is the bremsstrahlung fluence calculated by a Monte Carlo (MC) simulation code, which we hereafter refer to as an MC-γ fluence. The derivation is provided in the Appendix.

For obtaining MC-γ fluences, we simulated electron beams of 1-mm diameter from 20 to 70 MeV at 1-MeV intervals using PHITS [51] and EGS [52] MC programs. Here the lowest electron beam energy, 20 MeV, was set considering the 8.29-MeV threshold and 14-MeV peak resonance energies of ^{100}Mo$(\gamma, n)^{99}$Mo [45], and the fact that photons lose their energies while traversing a Mo target. The electron beams were simulated to impinge on a $^{\mathrm{nat}}$W converter for generating bremsstrahlung photons. The photons then collided with $^{\mathrm{enr}}$Mo, a Mo target enriched to 95% in ^{100}Mo, placed immediately behind the $^{\mathrm{nat}}$W converter. The dimensions of this target assembly are summarized in Table II.

As for the ^{100}Mo$(\gamma, n)^{99}$Mo cross section, we used the one contained in the nuclear data library TENDL-2009

TABLE II. Geometrical parameters of the target assembly.

Target	Shape	Parameter (cm)		Volume (cm^3)
$^{\mathrm{nat}}$W for $^{\mathrm{nat}}$W(e,γ)	Disk	Radius	2	1.257
		Thickness	0.1	
$^{\mathrm{enr}}$Mo for ^{100}Mo(γ,n)	Truncated cone	Lower radius	0.15	0.495
		Upper radius	0.6	
		Height	1	

[45], coplotted with several MC-γ fluences in Fig. 3. The coplotting shows the influence of electron beam energy on the amount of bremsstrahlung photons having energies close to the giant resonance of ^{100}Mo$(\gamma,n)^{99}$Mo.

Figure 4 illustrates the ^{99}Mo activity obtained from Eq. (5), revealing that, at least over the given energy range, the yield of ^{99}Mo increases almost linearly with electron beam energy at a faster rate with a longer irradiation time.

Next, we generated a three-dimensional (3D) ^{99}Mo activity plot and its two-dimensional (2D) projection, shown in Figs. 5(a) and 5(b), respectively. While the 3D graph provides an overview of the dependence of ^{99}Mo activity on t_{irr} and E_e, the 2D contour map suggests that t_{irr} can be a decisive criterion in choosing the final electron beam energy. For example, to acquire a ^{99}Mo activity of 1.25 GBq μA^{-1}, which equals the fifth contour line from the bottom, the required beam-on time of the 20-MeV electron beam is found to be 273 h, whereas the 25-MeV one would complete the same task in only 75 h. If the same activity is obtained at a shorter irradiation time, more frequent ^{99}Mo production runs can be performed and less thermal energy will be accumulated in the target module, implying that a high final beam energy is preferable.

Also desirable is a high beam current, as the ^{99}Mo yield is directly proportional to beam current. To realize a compact, high-energy and high-current electron linac, however, both a high accelerating gradient and a high-power rf source can become necessary, which can in turn increase the rf power costs [38,53]; we stress that reducing the capital costs is crucial for realizing the decentralized ^{99}Mo/^{99m}Tc supply, because this will demand multiple electron-linac facilities. Besides, the induced radioactivity in and around beam line components, which can increase with electron beam energy [54,55], was another consideration for the choice of final beam energy.

Considering together these factors requiring different final beam energies, we decided to set the final beam energy such that it provides adequate ^{99}Mo productivity at reasonable capital costs and, finally, selected 35 MeV: in Fig. 5(b), the contour-line curvatures up to around the eighth contour line from the bottom, or 2 GBq μA^{-1}, are satisfactorily small at 35 MeV, above which energy no drastic increase in the ^{99}Mo activity is observed. Besides, the 35-MeV final beam energy falls within those of previous electron-linac approaches found in Refs. [23–27,32], 30–60 MeV.

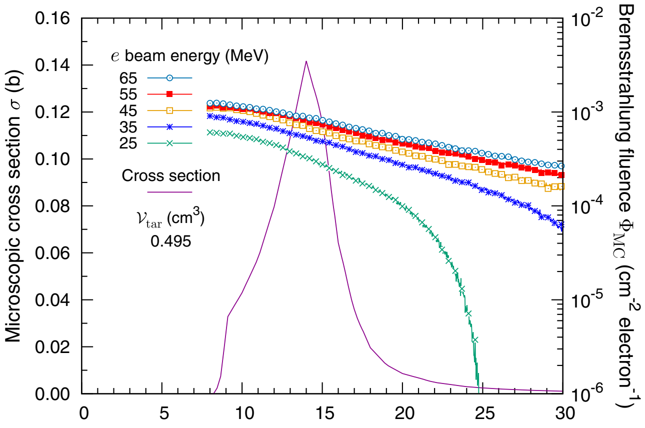

FIG. 3. Solid line, associated with the left y-axis: microscopic cross section of ^{100}Mo$(\gamma,n)^{99}$Mo. Lines with points, associated with the right y-axis: bremsstrahlung fluences simulated at different electron (e) beam energies.

C. rf design

1. X-band rf power

Equation (5) shows that considering the ^{99}Mo yield, an X-band rf source exhibiting a reasonably high duty cycle is desirable. We thus decided to use E37113 of Toshiba

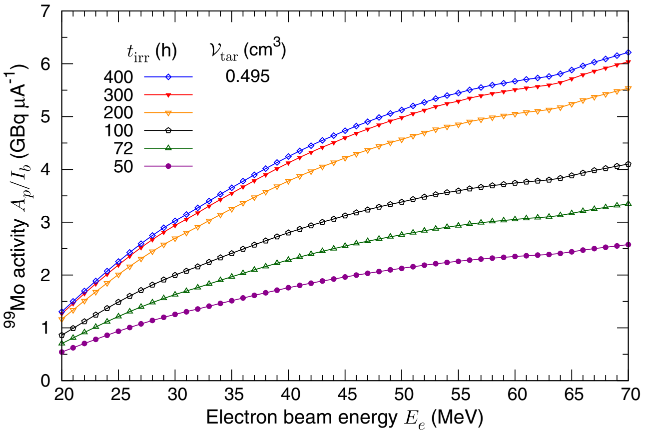

FIG. 4. ^{99}Mo activity calculated from Eq. (5) at different irradiation times, varying with electron beam energy.

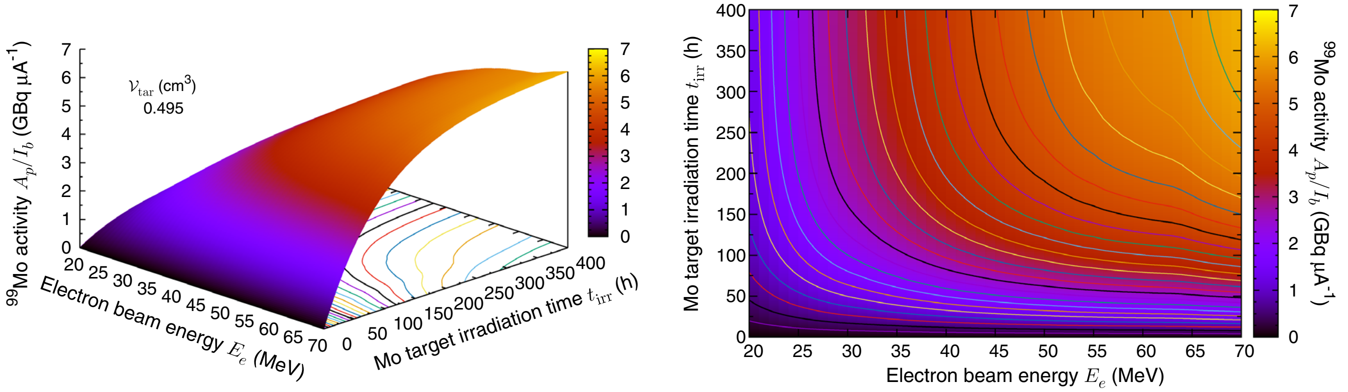

(a) (b)

FIG. 5. (a) ^{99}Mo activity calculated from Eq. (5), varying with electron beam energy and $^{\mathrm{enr}}$Mo target irradiation time; and (b) its two-dimensional projection. The contour lines begin at 0.25 $\mathrm{GBq}\,\mu\mathrm{A}^{-1}$ from the bottom and are spaced by 0.25 $\mathrm{GBq}\,\mu\mathrm{A}^{-1}$.

Electron Tubes & Devices Co., Ltd. [56], a pulsed klystron designed to output a 6-MW peak power of 11.9942-GHz rf with a duty cycle of $5\ \mu\mathrm{s} \times 400\ \mathrm{pps} = 0.002$, or 0.2%. Using two of them will then provide a 12-MW peak or 24-kW average *X*-band rf power.

The klystron-output *X*-band rf power P_k, however, is considerably reduced before fed into the accelerating structure, owing largely to the high-loss nature of high-frequency microwaves in waveguides. This reduction was quantified by the attenuation constant in rectangular waveguides per unit length [57],

$$\alpha_{\mathrm{att}} = \frac{1}{wh\sigma_e\delta_s k_0 k_z}\sqrt{\frac{\varepsilon_0}{\mu_0}}(k_0^2 w + 2k_c^2 h)\frac{20}{\ln 10},$$

with the parameters given in Table III. The result was $0.0984\ \mathrm{dB\,m^{-1}}$; a 5-m long WR-90 waveguide would then consume 0.492 dB. Also reducing the *X*-band rf power before the cavities is summarized in Table IV. In total, the peak *X*-band rf powers which can be delivered to the accelerating modules AM-A and AM-B, denoted by P_0's, would be 4.008 and 4.197 MW, respectively.

2. Side-coupled structure

By displacing its unexcited coupling cavities off the beam line [43], an SCS exhibits a high effective shunt impedance per unit length R_{sh} that is characteristic of the π mode, yet operating in the $\pi/2$ mode which offers field stability [38,53].

For designing an SCS, we parametrized its accelerating cavity and adjusted the gap length g using SUPERFISH [59], a simulation package of electromagnetic (EM) field solvers, such that R_{sh} becomes sufficiently high. Figure 6 plots this R_{sh} as a function of g, or $R_{\mathrm{sh}}(g)$, showing that $R_{\mathrm{sh}}(7.5\ \mathrm{mm}) = 152.04\ \mathrm{M\Omega/m}$ is the largest. The cavity structure is depicted in Fig. 7.

The coupling slots in Fig. 7, however, were omitted in the SUPERFISH simulations, which could lead to reductions in the unloaded quality factor Q_0, and R_{sh}. Accordingly, we decreased the SUPERFISH results of all SCSs by 20%, and those of the first SCS further by 10%, as this will contain the buncher section. The resultant cavity figures of merit are summarized in Table VI.

On the other hand, as the beam aperture diameter is as narrow as 4 mm, even a small transverse deflection of the beam will lead to its collision with the disk and hence BBU

TABLE III. Parameters of α_{att} at $f = 11.9942$ GHz.

	Symbol and meaning	Value	Unit
w	WR-90[a] cross-sectional width	22.86×10^{-3}	m
h	WR-90[a] cross-sectional height	10.16×10^{-3}	m
σ_e	Copper electrical conductivity[b]	5.813×10^{7}	$\mathrm{S\,m^{-1}}$
δ_s	Skin depth	5.994×10^{-7}	m
k_0	Vacuum wave number	251.334	$\mathrm{m^{-1}}$
k_z	z-direction wave number	210.434	$\mathrm{m^{-1}}$
k_c	Cutoff wave number	137.428	$\mathrm{m^{-1}}$
ε_0	Vacuum permittivity	8.854×10^{-12}	$\mathrm{F\,m^{-1}}$
μ_0	Vacuum permeability	$4\pi \times 10^{-7}$	$\mathrm{H\,m^{-1}}$

[a] Defined by the Electronic Industries Alliance designations for standard rectangular waveguides.
[b] Ref. [58].

TABLE IV. rf power losses in the X-band microwave circuit.

			rf power loss (dB)	
Item consuming rf power	Unit loss (dB)	Number of items	AM-A	AM-B
α_{att} (waveguide)	0.0984/m	5	0.492	0.492
Waveguide flange	0.03/item	10	0.3	0.3
Circulator	0.5/item	1	0.5	0.5
rf window	0.03/item	2	0.06	0.06
Power distributor	0.2/item	1	0.2	0.2
Phase shifter	0.2/item	1[a]	0.2	0
Total rf power loss (dB)			1.752	1.552
Klystron-output peak rf power P_k (MW)			6	6
Structure-input peak rf power P_0 (MW)			4.008	4.197

[a] In the AM-A only.

[38]. Also, high impedances of the dipole modes can result from the nose cones, in which case BBU occurs at a relatively low beam current. To reduce BBU, a focusing coil will surround the SCS-1, in which the beam has low energy and hence is more affected by the dipole modes.

3. Output beam current

The steady-state accelerating voltage in a beam-loaded standing-wave structure is given by [38,44,60]

$$V_{\mathrm{st}} = \sqrt{P_0 R_{\mathrm{sh}} L}\left(\frac{2\sqrt{\beta}}{1+\beta}\right) - \frac{R_{\mathrm{sh}} L I_b}{1+\beta}, \tag{6}$$

where β is the waveguide-to-cavity coupling coefficient, and L is the structure length.

Inserting Eq. (6) into the power delivered to electron beams $P_b = V_{\mathrm{st}} I_b$, we obtain the rf-to-beam efficiency

$$\eta = \frac{P_b}{P_0} = \frac{2V_{\mathrm{st}}\sqrt{\beta P_0 R_{\mathrm{sh}} L} - V_{\mathrm{st}}^2(1+\beta)}{P_0 R_{\mathrm{sh}} L}. \tag{7}$$

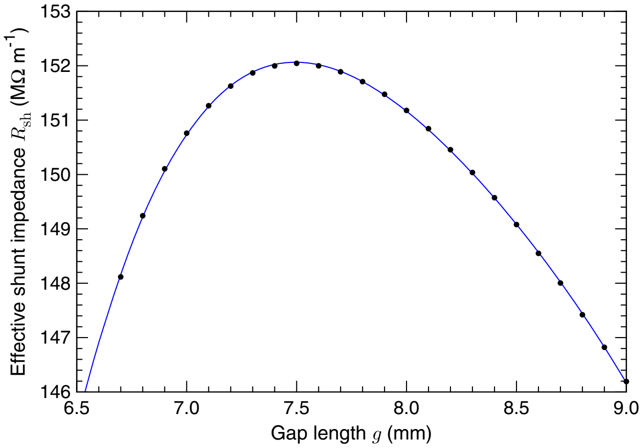

FIG. 6. SUPERFISH-calculated effective shunt impedance per unit length as a function of accelerating cavity gap length.

Setting $V_{\mathrm{st}} = 17.5$ MV in Eq. (7) so that two klystrons can achieve the 35-MV goal axial voltage, assuming a typical $\beta = 2.5$ [61], and using the P_0 of AM-B and R_{sh} of SUPERFISH given in Tables IV and VI, respectively, we are left with $\eta = \eta(L)$, graphed in Fig. 8. Although $\eta(2.939\mathrm{m}) = 0.714$ was found to be the highest, we opted for $L = 2$ m to keep the linac compact, at which η is still as high as 0.682.

Since, however, manufacturing a 2-m long SCS at $f = 11.9942$ GHz is a technical challenge, we decided to halve the SCS and combine the fragments into one module. Namely, one accelerating module fed by one X-band klystron will consist of two 1-m long SCSs, and two such modules will be used.

As $L = 1$ m was determined, Eq. (6) reduced to $V_{\mathrm{st}}(I_b)$, but now with P_0's and R_{sh}'s of the respective SCSs. Figure 9 shows the V_{st}'s of individual SCSs and their sum, from which we can find

$$\sum_{m=1}^{4} V_{\mathrm{st},m}(158\ \mathrm{mA}) = 35\ \mathrm{MV},$$

where m is the SCS index; since the beam energy gain is $\Delta W = qV_{\mathrm{st}}$ where q is the elementary charge, the peak

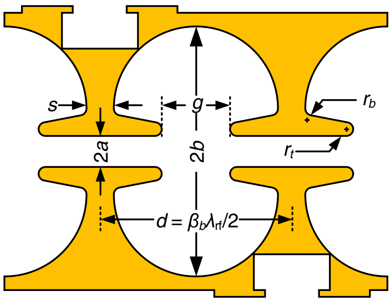

FIG. 7. Accelerating cavity of the SCS. $\beta_b = 1$ is the beam velocity normalized to the speed of light c; other parameters are given in Table V.

TABLE V. Design parameters of Fig. 7.

Symbol	Meaning	Value (mm)
λ_{rf}	Wavelength of 11.9942-GHz rf	25
$2a$	Beam aperture diameter	4
$2b$	Cavity diameter	19.798
d	Cavity length	12.5
s	Disk thickness	2
g	Gap length	7.5
r_t	Nose cone tip radius	0.5
r_b	Nose cone base radius	1.2

TABLE VI. Cavity figures of merit obtained from SUPERFISH.

Figure of merit	SUPERFISH	SCS-1	SCS-2 to SCS-4
Ratio to SUPERFISH	1.00	0.72	0.80
Q_0	8446.78	6081.68	6757.42
R_{sh} (MΩ/m)	152.04	109.47	121.63

beam energy and current are 35 MeV and 158 mA, respectively. Taking into account the 0.2% duty cycle of E37113, then, the average beam current and power are 316 μA and 11.06 kW, respectively.

D. Beam dynamics study

While the rf design study provided approximate output beam energy and current, a number of possible physical phenomena were overlooked, an example being the space-charge effects. We therefore performed particle tracking simulations using GPT [62], of which the EM field maps were provided by SUPERFISH.

Figure 10 [47], the counterpart of Fig. 9, shows that at the beam line exit, the peak beam current is approximately 130 mA at the goal beam energy of 35 MeV. Considering the 0.2% klystron duty cycle, then, the average beam current and power are 260 μA and 9.1 kW, respectively. This beam current is smaller than that obtained from Eq. (6) by a factor of 1.215, which we attribute to the limited configuration input to GPT: in the simulation runs, we failed to place the second pair of quadrupole magnets between the SCS-3 and SCS-4 (see Fig. 2), owing to a technical problem in the usage of the code. If such a focusing element can be correctly set in the simulation, a higher beam current can result.

In Fig. 11 [47] we show the GPT-calculated electron beam size. The beam diameter at the beam exit is found to be less than 0.8 mm, close to the 1-mm one used in the MC simulations.

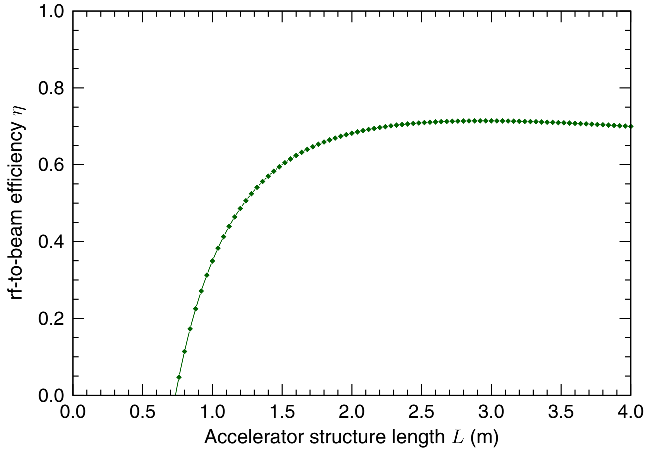

FIG. 8. rf-to-beam power efficiency as a function of accelerator structure length.

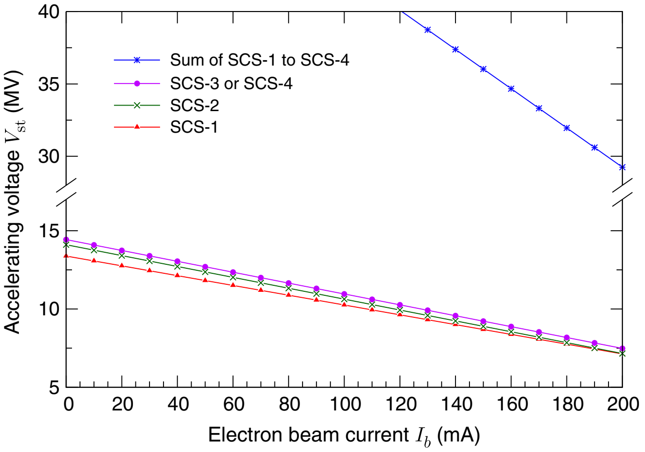

FIG. 9. Accelerating voltage and beam current in the SCSs given by Eq. (6).

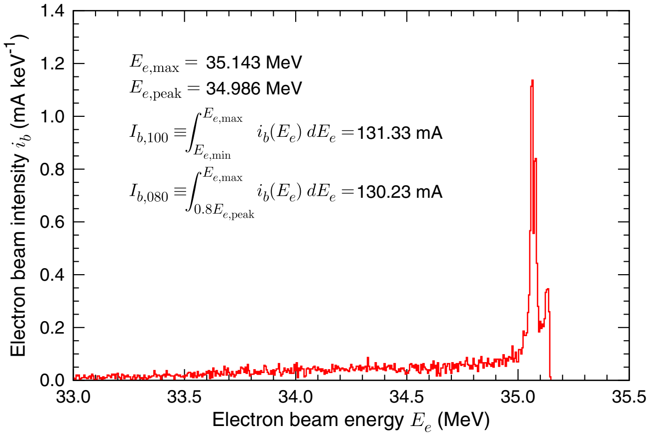

FIG. 10. Beam energy and current at the beam exit $z = 5$ m obtained from GPT; i_b, beam intensity per keV; $E_{e,\mathrm{min}}$ and $E_{e,\mathrm{max}}$, the lowest and highest beam energies, respectively; $E_{e,\mathrm{peak}}$, the beam energy at which i_b is the largest.

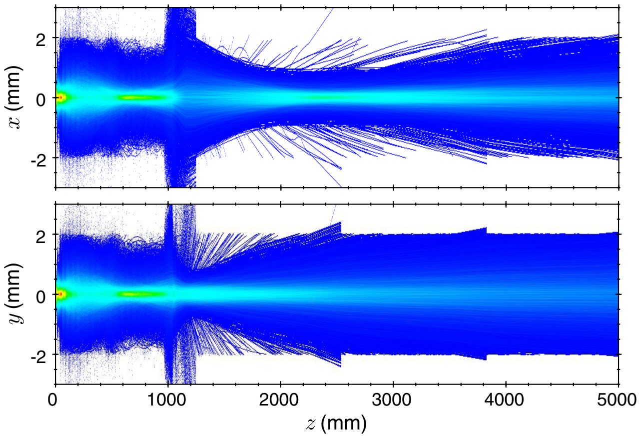

FIG. 11. Beam size in (upper) xz- and (lower) yz-planes.

III. ^{99}Mo/^{99m}Tc SUPPLY CAPACITY OF THE X-BAND ELECTRON LINAC

Finally, for examining the adequacy of the calculated beam energy and current, we calculated the expected ^{99}Mo/^{99m}Tc yields, and eventually the number of designed electron linacs necessary for a specific country to be self-sufficient in ^{99}Mo/^{99m}Tc. We selected Japan as the country of interest because, despite being the world's second-largest ^{99m}Tc radiopharmaceutical consumer [63], Japan has neither domestic nor neighboring large-scale ^{99}Mo production facilities [19,63], and therefore is severely affected by ^{99}Mo supply disruptions [19].

A. One-day Bq for ^{99}Mo pricing

In the ^{99}Mo/^{99m}Tc market, a special unit of activity referred to as six-day Ci is used for pricing ^{99}Mo and, by extension, representing the collective demand and supply of ^{99}Mo/^{99m}Tc [13,64]. Being essentially the same unit as Ci ($1\ \mathrm{Ci} = 3.7 \times 10^{10}$ Bq), six-day Ci signifies the activity of ^{99}Mo that will remain six days after it is separated from an irradiated ^{235}U target [13]. This concept is valid in the current ^{99}Mo/^{99m}Tc market structure, where ^{99}Mo is produced and processed in a small number of countries and distributed throughout the world, during which up to six days elapse.

In contrast, under the decentralized ^{99}Mo/^{99m}Tc supply scheme, the postirradiation tasks would take, at least in Japan, no longer than one day. We hence propose using a new unit for pricing ^{99}Mo, called one-day Bq, which takes into account both the shortened time scale and the SI derived unit.

Unlike six-day Ci, however, one-day Bq fails to quantify the joint ^{99}Mo/^{99m}Tc demand and supply, because data relating the activity of photonuclear-produced ^{99}Mo and that of the extractable ^{99m}Tc are yet to be sufficient. We instead used the ^{99m}Tc activity, which necessitated estimating the ^{99m}Tc demand and modeling the activities of photonuclear-produced ^{99}Mo/^{99m}Tc.

B. ^{99m}Tc demand in Japan

While emerging ^{99}Mo/^{99m}Tc markets have been growing and are expected to grow further at a rate of 3%–5% for the next five years [3,65], Japan, classified as a mature market [64], has seen declines in its ^{99m}Tc consumption over the past few years: in 2002, about one-million ^{99m}Tc-based medical scans were carried out [66], but it dropped to 0.9 million in 2008 [63], and to 0.7 million in 2012 [67].

We attribute these ^{99m}Tc market downturns to the recent series of ^{99}Mo/^{99m}Tc supply disruptions brought about by the aging of the foreign reactors [63], and therefore expect that the Japanese ^{99m}Tc demand will rise, so long as a reliable ^{99}Mo production source, including the designed X-band electron linac, is secured. For this reason, we adopted the 2002 one-million ^{99m}Tc scans, the highest figure among those mentioned above, as the annual ^{99m}Tc demand in this study; using the 740-MBq average dose of ^{99m}Tc radiopharmaceuticals [15,16,24], the ^{99m}Tc weekly demand was therefore assumed to be $D_{d,\mathrm{week}} = 14.23\ \mathrm{TBq\,week}^{-1}$.

C. Radioactivity model of photonuclear-produced ^{99}Mo/^{99m}Tc

We begin with setting a system of the modified Bateman equation for ^{99}Mo, or Eq. (1), and an original one for ^{99m}Tc:

$$\begin{pmatrix} N'_p(t_{\mathrm{irr}}) \\ N'_d(t_{\mathrm{irr}}) \end{pmatrix} = \begin{pmatrix} -\lambda_p & 0 \\ \lambda_p & -\lambda_d \end{pmatrix} \begin{pmatrix} N_p(t_{\mathrm{irr}}) \\ N_d(t_{\mathrm{irr}}) \end{pmatrix} + \begin{pmatrix} \mathcal{R}_{\mathrm{tar}} \\ 0 \end{pmatrix}, \tag{8}$$

where the prime ($'$) denotes the first derivative.

Solving the eigenvalue-eigenvector problem, we have

$$L_p = -\lambda_p, \quad X_p = \begin{pmatrix} 1 \\ \frac{\lambda_p}{\lambda_d - \lambda_p} \end{pmatrix},$$
$$L_d = -\lambda_d, \quad X_d = \begin{pmatrix} 0 \\ 1 \end{pmatrix}, \tag{9}$$

where L is the eigenvalue of $\left(\begin{smallmatrix} -\lambda_p & 0 \\ \lambda_p & -\lambda_d \end{smallmatrix}\right)$, and X is the eigenvector corresponding to L.

Using Eq. (9), we obtain the general solutions of Eq. (8):

$$\begin{aligned} N_p(t_{\mathrm{irr}}) &= \left(\frac{1 - e^{-\lambda_p t_{\mathrm{irr}}}}{\lambda_p}\right)\mathcal{R}_{\mathrm{tar}} + N_p(0)e^{-\lambda_p t_{\mathrm{irr}}}, \\ N_d(t_{\mathrm{irr}}) &= \left(\frac{\lambda_p N_p(0) - \mathcal{R}_{\mathrm{tar}}}{\lambda_d - \lambda_p}\right)e^{-\lambda_p t_{\mathrm{irr}}} \\ &\quad + \left[N_d(0) + \left(\frac{\lambda_p \mathcal{R}_{\mathrm{tar}} - \lambda_d \lambda_p N_p(0)}{\lambda_d(\lambda_d - \lambda_p)}\right)\right]e^{-\lambda_d t_{\mathrm{irr}}} \\ &\quad + \frac{\mathcal{R}_{\mathrm{tar}}}{\lambda_d}, \end{aligned}$$

or, since $A_i(t) = \lambda_i N_i(t)$,

$$
\begin{aligned}
A_p(t_{\mathrm{irr}}) &= (1-e^{-\lambda_p t_{\mathrm{irr}}})\mathcal{R}_{\mathrm{tar}} + A_p(0)e^{-\lambda_p t_{\mathrm{irr}}},\\
A_d(t_{\mathrm{irr}}) &= \frac{\lambda_d}{\lambda_d-\lambda_p}A_p(0)(e^{-\lambda_p t_{\mathrm{irr}}}-e^{-\lambda_d t_{\mathrm{irr}}}) + A_d(0)e^{-\lambda_d t_{\mathrm{irr}}} + \left[1-\left(\frac{\lambda_d e^{-\lambda_p t_{\mathrm{irr}}}-\lambda_p e^{-\lambda_d t_{\mathrm{irr}}}}{\lambda_d-\lambda_p}\right)\right]\mathcal{R}_{\mathrm{tar}}.
\end{aligned}
$$

Generally, the ^{99}Mo activity is zero before Mo target irradiation begins, in which case the initial conditions $A_p(0) = A_d(0) = 0$ hold. In addition, we take into account the ^{99}Mo branching fraction for the β^- decay to ^{99m}Tc, B, and apply Eq. (2) and the MC-simulation-oriented approach found in the Appendix. We then obtain the during-irradiation activities of ^{99}Mo and ^{99m}Tc, respectively:

$$A_p(t_{\mathrm{irr}}) = [1-\exp(-\lambda_p t_{\mathrm{irr}})]\mathcal{V}_{\mathrm{tar}} I_b \int_{E_{\gamma,\mathrm{min}}}^{E_{\gamma,\mathrm{max}}} \Phi_{\mathrm{MC}}(E_\gamma)\Sigma(E_\gamma)dE_\gamma, \tag{10a}$$

$$A_d(t_{\mathrm{irr}}) = B\left\{\left[1+\frac{\lambda_d}{\lambda_p-\lambda_d}\exp(-\lambda_p t_{\mathrm{irr}}) + \frac{\lambda_p}{\lambda_d-\lambda_p}\exp(-\lambda_d t_{\mathrm{irr}})\right]\mathcal{V}_{\mathrm{tar}} I_b \int_{E_{\gamma,\mathrm{min}}}^{E_{\gamma,\mathrm{max}}} \Phi_{\mathrm{MC}}(E_\gamma)\Sigma(E_\gamma)dE_\gamma\right\}. \tag{10b}$$

If $\binom{\mathcal{R}_{\mathrm{tar}}}{0} = 0$, Eq. (8) reduces to

$$\begin{pmatrix} N'_p(t_{\mathrm{dec}}) \\ N'_d(t_{\mathrm{dec}}) \end{pmatrix} = \begin{pmatrix} -\lambda_p & 0 \\ \lambda_p & -\lambda_d \end{pmatrix}\begin{pmatrix} N_p(t_{\mathrm{dec}}) \\ N_d(t_{\mathrm{dec}}) \end{pmatrix}, \tag{11}$$

where t_{dec} signifies the time during which ^{99}Mo is no longer produced and decays only.

Noting that Eq. (9) holds also for Eq. (11), and using again $A_i(t) = \lambda_i N_i(t)$, we now obtain the postirradiation activities of ^{99}Mo and ^{99m}Tc, respectively:

$$A_p(t_{\mathrm{dec},n}) = \begin{cases} A_p(0)\exp(-\lambda_p t_{\mathrm{tra}}), & n=1 \\ A_p(0)\exp(-\lambda_p t_{\mathrm{dec},n}), & n\geq 2 \end{cases} \tag{12a}$$

$$A_d(t_{\mathrm{dec},n}) = \begin{cases} B\left\{\frac{\lambda_d}{\lambda_d-\lambda_p}A_p(0)[\exp(-\lambda_p t_{\mathrm{tra}})-\exp(-\lambda_d t_{\mathrm{tra}})]\right\} + A_d(0)\exp(-\lambda_d t_{\mathrm{tra}}), & n=1 \\ B\left\{\frac{\lambda_d}{\lambda_d-\lambda_p}A_p(0)[\exp(-\lambda_p t_{\mathrm{dec},n})-\exp(-\lambda_d t_{\mathrm{dec},n})]\right\} + A_d(0)\exp(-\lambda_d t_{\mathrm{dec},n}), & n\geq 2, \end{cases} \tag{12b}$$

where n is the ordinal number of ^{99m}Tc elution and hence $t_{\mathrm{dec},n}$ the time elapsed between elution runs $n-1$ and n, and t_{tra} is the time required for transporting ^{99}Mo-loaded ^{99m}Tc generators to end users. The initial conditions are

$$
\begin{aligned}
A_p(t_{\mathrm{dec},n}=0) &= \begin{cases} (1-\kappa)A_p(t_{\mathrm{EOP}}), & n=1 \\ A_p(t_{\mathrm{dec},n-1}), & n\geq 2 \end{cases}\\
A_p(t_{\mathrm{EOP}}) &= A_p(t_{\mathrm{EOI}})\exp(-\lambda_p t_{\mathrm{pro}}),\\
A_d(t_{\mathrm{dec},n}=0) &= \begin{cases} (1-\kappa)A_d(t_{\mathrm{EOP}}), & n=1 \\ (1-\zeta)A_d(t_{\mathrm{dec},n-1}), & n\geq 2 \end{cases}\\
A_d(t_{\mathrm{EOP}}) &= B\left\{\frac{\lambda_d}{\lambda_d-\lambda_p}A_p(t_{\mathrm{EOI}})[\exp(-\lambda_p t_{\mathrm{pro}})-\exp(-\lambda_d t_{\mathrm{pro}})]\right\} + A_d(t_{\mathrm{EOI}})\exp(-\lambda_d t_{\mathrm{pro}}),
\end{aligned} \tag{13}
$$

where t_{EOI} is the time at the end of irradiation (EOI), t_{pro} is the time during which the irradiated Mo target is cooled and chemically processed, t_{EOP} is the time at the end of chemical processing (EOP), κ is the ratio of ^{99}Mo lost at EOP, and ζ is the ^{99m}Tc elution efficiency.

Figures 12 and 13 illustrate the during-irradiation and postirradiation ^{99}Mo/^{99m}Tc activities calculated from Eqs. (10), (12), and (13) with the following values: (1) $\mathcal{V}_{\mathrm{tar}} = 0.495$ cm^3 given in Table II; (2) $I_b = 260$ μA of the beam dynamics study; (3) $\Phi_{\mathrm{MC}}(E_\gamma)$ at $E_e = 35$ MeV

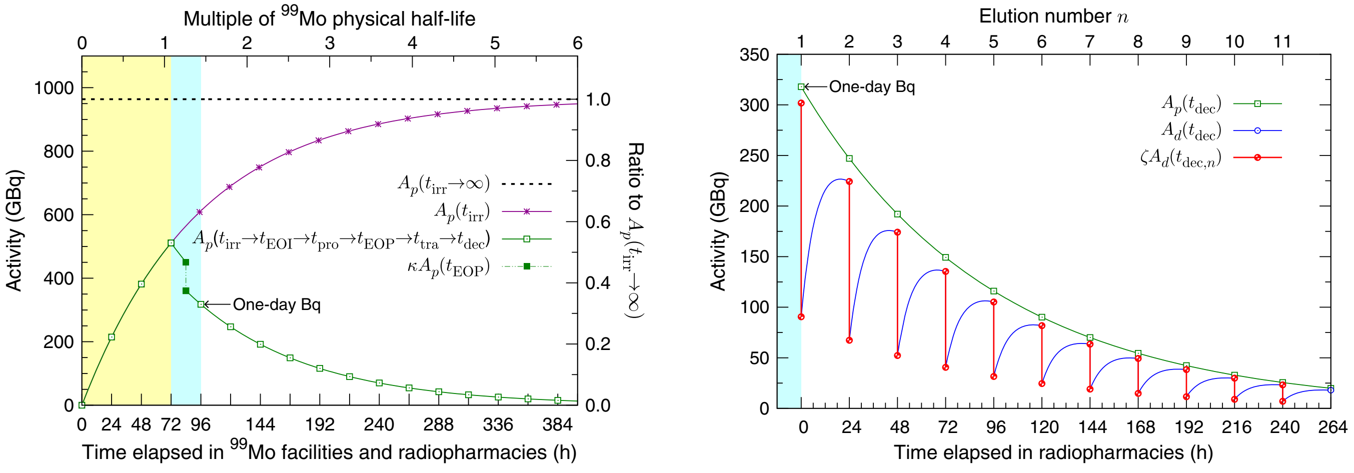

(a) (b)

FIG. 12. (a) Modeled activities of photonuclear-produced ^{99}Mo and (b) its ^{99m}Tc eluates.

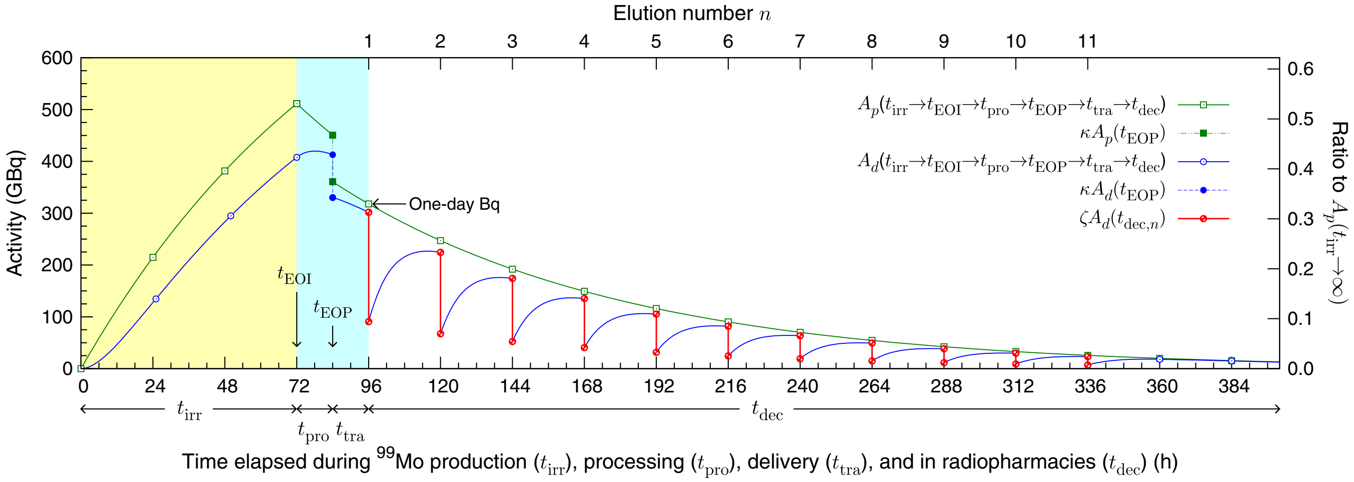

FIG. 13. Comprehensive view of the modeled activities of photonuclear-produced ^{99}Mo/^{99m}Tc.

plotted in Fig. 3; (4) $\Sigma(E_\gamma)$ of the TENDL-2009; (5) $B = 0.875$ the known value [5,12]; (6) $\kappa = 0.2$ assumed based on $\kappa \leq 0.15$ of the fission-^{99}Mo production scheme [16]; and lastly (7) $\zeta = 0.7$ based on $\zeta \geq 0.9$ of ^{99m}Tc generators developed for use with ^{99}Mo having low specific activity (LSA) [13,68]. The higher κ and lower ζ allow avoiding underestimation. As for the $t_{\rm EOI}$ and ^{99m}Tc elution conditions, explanations are provided below.

First, in the interest of efficient routine production of ^{99}Mo, we selected $t_{\rm irr} = 72$ h as the $t_{\rm EOI}$, by which two production runs can be performed per week, and at which the ratio of A_p to the ^{99}Mo saturation activity $A_{p,{\rm sat}} \equiv A_p(t_{\rm irr} \to \infty)$ is as high as

$$\frac{1-\exp(-\frac{\ln 2}{T_{{\rm phy},p}}1.09T_{{\rm phy},p})}{1-\lim_{t_{\rm irr}\to+\infty}\exp(-\lambda_p t_{\rm irr})} \approx 0.53, \tag{14}$$

where $T_{{\rm phy},p} = \frac{\ln 2}{\lambda_p}$ is the 66-hour ^{99}Mo physical half-life. Equation (14) can be derived from Eq. (10a), and is also shown graphically in Fig. 12(a).

On the other hand, we set the intervals between successive ^{99m}Tc elutions, or $t_{{\rm dec},n}$, to 24 h, which allows simple elution scheduling and provides as high A_d as $0.91A_p$; this ratio can be seen visually in Figs. 12(b) and 13, and quantitatively in Eq. (12). In addition, we assumed the ^{99m}Tc generator life to be ten days, after which ^{99}Mo that is loaded in a ^{99m}Tc generator loses most of its initial activity:

$$\exp\left(-\frac{\ln 2}{T_{{\rm phy},p}}3.64T_{{\rm phy},p}\right)A_p(t_{{\rm dec},1}) \approx 0.08A_p(t_{{\rm dec},1}),$$

which can be obtained from Eq. (12a).

Also important is to discard the ^{99m}Tc eluate at $n = 1$, because a substantial portion of ^{99m}Tc decays to its ground state (^{99g}Tc) en route to radiopharmacies; as its chemistry is almost identical to that of ^{99m}Tc, ^{99g}Tc degrades the quality of ^{99m}Tc radiopharmaceuticals [33,35].

Finally, as two sets of 72-h Mo target irradiation can be performed per week, the weekly ^{99m}Tc supply of the 35-MeV and 260-μA *X*-band electron linac would be

$$A_{d,\mathrm{week}} = 2\left[\zeta \sum_{n=2}^{11} A_d(t_{\mathrm{dec},n})\right] = 1.295\ \mathrm{TBq\,week^{-1}}, \quad (15)$$

where $\zeta A_d(t_{\mathrm{dec},n})$'s are described in Figs. 12(b) and 13. It follows from Eq. (15) that

$$\frac{A_{d,\mathrm{week}}}{2[A_p(t_{\mathrm{dec},1})]} = 2.037,$$

meaning that the ^{99m}Tc yield of a ^{99m}Tc generator is approximately twice the loaded ^{99}Mo activity.

Dividing the weekly ^{99m}Tc demand in Japan addressed in Sec. III B by Eq. (15), and using the ceiling function to prevent underestimation, we arrive at

$$\left\lceil \frac{D_{d,\mathrm{week}}}{A_{d,\mathrm{week}}} \right\rceil = \left\lceil \frac{14.23\ \mathrm{TBq\,week^{-1}}}{1.295\ \mathrm{TBq\,week^{-1}}} \right\rceil = 11, \quad (16)$$

which is the number of designed *X*-band electron linacs that can meet the national demand for ^{99m}Tc in Japan.

Similarly, by substituting the weekly ^{99m}Tc demand of a specific country into the numerator of Eq. (16), the number of designed *X*-band electron linacs required for their ^{99m}Tc self-sufficiency can be estimated.

IV. DISCUSSION

A. Operating frequency

Focusing more on the decentralization of ^{99}Mo/^{99m}Tc supply chain than on the ^{99}Mo yield, we selected *X*-band rf as the operating frequency, at which a satisfactory beam current was calculated. If, however, electron linacs operating at the subharmonic rf's are designed to output beam energy and current similar to those of the *X*-band one with better stability at an acceptable cost of compactness, the subharmonic rf's can become more advantageous. Conversely, if the *X*-band electron linac is optimized to provide a higher beam current at the same dimensions or a more compact size at the same beam current, the selection of *X*-band rf can be justified. One of the future studies is therefore to compare electron linacs of different operating frequencies exhibiting similar output beam energies and currents, with emphasis on the operational stability and cost effectiveness.

B. Final beam energy and current

The energy and current of electron beams are one of the major parameters that affect the ^{99}Mo yield. In this study, we set 35 MeV as the final beam energy by referring to the ^{99}Mo-yield contour map that we generated. The contour map revealed that the degree to which the irradiation time is reduced by increasing beam energy is dependent on both the ^{99}Mo yield in question and the starting beam energy to be increased. For example, when a unit ^{99}Mo activity of as small as 0.25 GBq μA^{-1} is to be obtained, even though the beam energy increases, no meaningful decrease in the irradiation time is observed. If 1.25 GBq μA^{-1} is the goal unit activity, on the other hand, increasing the beam energy from 20 to 25 MeV will save an irradiation time of 198 h, whereas doing so from 25 to 30 MeV will save 25 h only. These are shown by the density of ^{99}Mo-yield contour lines; as such, the dependence of ^{99}Mo yield on electron beam energy and Mo target irradiation time can now easily be seen on the same plane, which in turn can be used for setting the final beam energy of a ^{99}Mo-producing electron linac.

C. Target irradiation time

As electron beams having 35 MeV and 260 μA will impinge on the $^{\mathrm{nat}}$W disk and the resulting bremsstrahlung on the $^{\mathrm{enr}}$Mo target for 72 consecutive hours, a large fraction of the beam power will be deposited into the $^{\mathrm{nat}}$W-$^{\mathrm{enr}}$Mo target assembly as heat, for which a dedicated cooling system is necessary. Water convection is the simplest cooling method, but causes radiolysis and $^{\mathrm{enr}}$Mo target erosion [69]. Studies [69,70] have shown that a proper coolant can be helium (He) gas circulating throughout Mo disks, between which gaps are provided for the He flow. To realize the 72-h irradiation, we will design such an inert-gas-based target cooling system.

D. ^{99m}Tc elution from LSA ^{99}Mo

Specific activity of the radionuclide in question i is defined by [71,72]

$$A_{\mathrm{sp},i} \equiv \frac{A_i}{m_i + \sum_{j\neq i} m_j}, \quad (17)$$

where m_j is the mass of a stable or radioactive nuclide j coexisting with and isotopic to i. Equation (17) indicates that ^{99}Mo produced via ^{100}Mo$(\gamma, n)^{99}$Mo inevitably exhibits LSA, because both the reactant and product nuclides are the isotopes of molybdenum.

As the LSA of ^{99}Mo precludes the use of conventional alumina chromatography for ^{99m}Tc separation [3,13], several alternative methods [68,73,74] have been developed, upon which our assumed elution conditions, the time-invariant $\zeta = 0.7$ in particular, are based. This field, however, is still in its infancy, and therefore the elution conditions used in this study can all be changed as the technology progresses: certainly the value of ζ can be adjusted, ζ can become time dependent, and the number of elutions may not reach the used one, 11. Such changes will greatly affect the ^{99m}Tc supply capacity of the linac.

E. Comparison of photonuclear-produced ^{99}Mo

We were unable to compare our ^{99}Mo-yield estimate with those of the previous studies [23,25–27,29] for the following reasons: First, at an instant of irradiation time, the bremsstrahlung distribution in a target of $^{\mathrm{enr}}$Mo and hence the ^{99}Mo yield depend not only on the electron beam energy, but also on the compositions and dimensions of the $^{\mathrm{nat}}$W-$^{\mathrm{enr}}$Mo target assembly, which are not necessarily the same in different studies. Second, the ^{99}Mo-yield normalization is often inconsistent across studies. For instance, some authors [25–27] used the masses of involved Mo nuclides, beam power, and irradiation time to express their unit ^{99}Mo yields, while some, [23,29] including us, used the beam power only. If a standard allowing such comparison is established, more reliable yield estimations can be made in future works.

V. CONCLUSION

In an attempt to stabilize and reform the current centralized ^{99}Mo/^{99m}Tc supply scheme, we designed a 5-m long, 35-MeV, and 260-μA X-band electron linac by analyzing the microwave circuit and performing beam dynamics simulations. Subsequently, we mathematically modeled the yields of photonuclear-produced ^{99}Mo/^{99m}Tc putting emphasis on ^{99m}Tc, which suggests that by using 11 of the designed X-band electron linacs, Japan can become self-sufficient in ^{99}Mo/^{99m}Tc. This model is not confined to Japan and, as such, the number of X-band electron linacs necessary for a given country to achieve its self-sufficiency in ^{99}Mo/^{99m}Tc can be estimated by simply inserting their ^{99m}Tc weekly demand into the modeled equation.

As the vulnerability of the current global ^{99}Mo/^{99m}Tc supply chain is rooted in its small number of ^{99}Mo-producing reactor facilities available only in specific countries, the designed X-band electron linacs that are compact and hence easy to be installed throughout countries can be a promising alternative to the aging reactors.

ACKNOWLEDGMENTS

We are grateful to T. Ohtsuki and S. Sekimoto (Kyoto University) and K. Tatenuma (Kaken Inc.) for letting us join their experiments of L-band-electron-linac-based ^{99}Mo production and activated-carbon-based ^{99m}Tc separation, from which we could gain a deeper understanding of the overall process. We also thank T. Tadokoro (Hitachi Ltd.) for useful advice and discussion, and E. Tanabe (AET, Inc.) for research cooperation.

APPENDIX: SOLUTION OF A MODIFIED BATEMAN EQUATION ORIENTED TO MONTE CARLO SIMULATIONS

In its original form, Eq. (1) is written as

$$\frac{dN_p(t_{\mathrm{irr}})}{dt_{\mathrm{irr}}} = -\lambda_p N_p(t_{\mathrm{irr}}) + \phi(\mathbf{r}, E_\gamma)\Sigma(E_\gamma),$$

whose Laplace transform is

$$N_p(s) = \frac{\phi(\mathbf{r}, E_\gamma)\Sigma(E_\gamma)}{s(s+\lambda_p)} + \frac{N_p(t_{\mathrm{irr}})|_{t_{\mathrm{irr}}=0}}{s+\lambda_p}.$$

Taking the inverse transform yields the general solution

$$N_p(t_{\mathrm{irr}}) = \frac{(1-e^{-\lambda_p t_{\mathrm{irr}}})}{\lambda_p}\phi(\mathbf{r}, E_\gamma)\Sigma(E_\gamma) + N_p(0)e^{-\lambda_p t_{\mathrm{irr}}}.$$

In general, no ^{99}Mo exists before Mo target irradiation begins, from which it follows that $N_p(0) = 0$, yielding

$$N_p(t_{\mathrm{irr}}) = \frac{(1-e^{-\lambda_p t_{\mathrm{irr}}})}{\lambda_p}\phi(\mathbf{r}, E_\gamma)\Sigma(E_\gamma).$$

Multiplying by λ_p, we obtain

$$A_p(t_{\mathrm{irr}}) = [1-\exp(-\lambda_p t_{\mathrm{irr}})]\phi(\mathbf{r}, E_\gamma)\Sigma(E_\gamma). \tag{A1}$$

Because ϕ is measured and Σ is defined in the Mo target, we can rewrite Eq. (A1) as

$$A_p(t_{\mathrm{irr}}) = [1-\exp(-\lambda_p t_{\mathrm{irr}})] \times \int_{E_{\gamma,\min}}^{E_{\gamma,\max}} dE_\gamma \iiint_{\mathcal{V}_{\mathrm{tar}}} d\mathcal{V}_{\mathrm{tar}}\phi(\mathbf{r}, E_\gamma)\Sigma(E_\gamma),$$

or, by Eq. (3),

$$A_p(t_{\mathrm{irr}}) = [1-\exp(-\lambda_p t_{\mathrm{irr}})] \times \mathcal{V}_{\mathrm{tar}} \int_{E_{\gamma,\min}}^{E_{\gamma,\max}} dE_\gamma \phi(E_\gamma)\Sigma(E_\gamma). \tag{A2}$$

The bremsstrahlung fluence obtained from MC simulation platforms is [75]

$$\Phi_{\mathrm{MC}}(E_\gamma) = \frac{\Phi(E_\gamma)}{\text{source particle}}.$$

In addition, we use the definition of electric current and Eq. (4), finding

$$\phi(E_\gamma) = \Phi_{\mathrm{MC}}(E_\gamma) I_b.$$

Consequently, Eq. (A2) becomes

$$A_p(t_{\mathrm{irr}}) = [1 - \exp(-\lambda_p t_{\mathrm{irr}})] \times \mathcal{V}_{\mathrm{tar}} I_b \int_{E_{\gamma,\mathrm{min}}}^{E_{\gamma,\mathrm{max}}} dE_\gamma \Phi_{\mathrm{MC}}(E_\gamma) \Sigma(E_\gamma).$$

[1] National Research Council and Institute of Medicine, *Advancing Nuclear Medicine Through Innovation* (National Academies Press, Washington, DC, 2007).

[2] W. C. Eckelman, Unparalleled contribution of technetium-99*m* to medicine over 5 decades, JACC Cardiovasc. Imaging **2**, 364 (2009).

[3] International Atomic Energy Agency, *Non-HEU Production Technologies for Molybdenum-99 and Technetium-99m*, IAEA Nuclear Energy Series Vol. NF-T-5.4 (International Atomic Energy Agency, Vienna, 2013).

[4] T. P. Sanders, T. D. Sanders, and D. E. Kuhl, Optimizing the window of an Anger camera for ^{99m}Tc, J. Nucl. Med. **12**, 703 (1971).

[5] S. R. Cherry, J. A. Sorenson, and M. E. Phelps, *Physics in Nuclear Medicine*, 4th ed. (Saunders, Philadelphia, 2012).

[6] J. G. McAfee, C. F. Fueger, H. S. Stern, H. N. Wagner, and T. Migita, Tc^{99m} pertechnetate for brain scanning, J. Nucl. Med. **5**, 811 (1964).

[7] M. S. de Jong, Producing medical isotopes using x-rays, in *Proceedings of the 3rd International Particle Accelerator Conference, IPAC 2012, New Orleans, LA, 2012*, edited by V. Suller (IEEE, Piscataway, NJ, 2012), pp. 3177–3179.

[8] S. Liu and D. S. Edwards, ^{99m}Tc-labeled small peptides as diagnostic radiopharmaceuticals, Chem. Rev. **99**, 2235 (1999).

[9] S. Banerjee, M. R. A. Pillai, and N. Ramamoorthy, Evolution of Tc-99*m* in diagnostic radiopharmaceuticals, Semin. Nucl. Med. **31**, 260 (2001).

[10] International Atomic Energy Agency, *Technetium-99m Radiopharmaceuticals: Manufacture of Kits*, IAEA Technical Reports Series Vol. 466 (International Atomic Energy Agency, Vienna, 2008).

[11] C. K. Ross and W. T. Diamond, Predictions regarding the supply of ^{99}Mo and ^{99m}Tc when NRU ceases production in 2018, Phys. Canada **71**, 131 (2015).

[12] R. E. Boyd, Technetium-99*m* generators—The available options, Int. J. Appl. Radiat. lsot. **33**, 801 (1982).

[13] National Academies of Sciences, Engineering, and Medicine, *Molybdenum-99 for Medical Imaging* (National Academies Press, Washington, DC, 2016).

[14] D. Dick, Diversification of ^{99}Mo/^{99m}Tc supply, J. Nucl. Med. **55**, 875 (2014).

[15] OECD Nuclear Energy Agency, *The Supply of Medical Radioisotopes: An Economic Study of the Molybdenum-99 Supply Chain* (OECD, Paris, 2010).

[16] National Research Council, *Medical Isotope Production Without Highly Enriched Uranium* (National Academies Press, Washington, DC, 2009).

[17] B. Ponsard, Mo-99 supply issues: Status report and lessons learned, in *Proceedings of the 14th International Topical Meeting on Research Reactor Fuel Management, RRFM 2010, Marrakech, Morocco, 2010* (European Nuclear Society, Brussels, 2010).

[18] R. Van Noorden, Radioisotopes: The medical testing crisis, Nature (London) **504**, 202 (2013).

[19] OECD Nuclear Energy Agency, *The Supply of Medical Radioisotopes: Results from the Second Self-assessment of the Global* ^{99}Mo/^{99m}Tc *Supply Chain* (OECD, Paris, 2014).

[20] B. Guérin, S. Tremblay, S. Rodrigue, J. A. Rousseau, V. Dumulon-Perreault, R. Lecomte, J. E. van Lier, A. Zyuzin, and E. J. van Lier, Cyclotron production of ^{99m}Tc: An approach to the medical isotope crisis, J. Nucl. Med. **51**, 13N (2010).

[21] F. Bénard, K. R. Buckley, T. J. Ruth, S. K. Zeisler, J. Klug, V. Hanemaayer, M. Vuckovic, X. Hou, A. Celler, and J.-P. Appiah, Implementation of multi-curie production of ^{99m}Tc by conventional medical cyclotrons, J. Nucl. Med. **55**, 1017 (2014).

[22] Y. Nagai *et al.*, Generation of radioisotopes with accelerator neutrons by deuterons, J. Phys. Soc. Jpn. **82**, 064201 (2013).

[23] Y. Danon, R. Block, and J. Harvey, Production of Mo-99 using 30 MeV electrons and a Mo-100 target, Trans. Am. Nucl. Soc. **103**, 1081 (2010).

[24] C. Ross, R. Galea, P. Saull, W. Davidson, P. Brown, D. Brown, J. Harvey, G. Messina, R. Wassenaar, and M. de Jong, Using the ^{100}Mo photoneutron reaction to meet Canada's requirement for ^{99m}Tc, Phys. Canada **66**, 19 (2010).

[25] A. N. Dovbnya, V. V. Mytrochenko, V. I. Nikiforov, S. A. Perezhogin, V. A. Shevchenko, B. I. Shramenko, A. E. Tenishev, A. V. Torgovkin, and V. L. Uvarov, Two-channel mode of Mo-99 production at an electron accelerator, in *Proceedings of the 2nd International Particle Accelerator Conference, IPAC 2011, San Sebastián, Spain, 2011*, edited by C. Petit-Jean-Genaz (EPS-AG, Spain, 2011), pp. 3627–3629.

[26] V. N. Starovoitova, L. Tchelidze, and D. P. Wells, Production of medical radioisotopes with linear accelerators, Appl. Radiat. Isot. **85**, 39 (2014).

[27] R. Avagyan, A. Avetisyan, I. Kerobyan, and R. Dallakyan, Photo-production of ^{99}Mo/^{99m}Tc with electron linear accelerator beam, Nucl. Med. Biol. **41**, 705 (2014).

[28] K. Mang'era, K. Ogbomo, R. Zriba, J. Fitzpatrick, J. Brown, E. Pellerin, J. Barnard, C. Saunders, and M. de Jong, Processing and evaluation of linear accelerator-produced ^{99}Mo/^{99m}Tc in Canada, J. Radioanal. Nucl. Chem. **305**, 79 (2015).

[29] A. D. Roberts, C. G. R. Geddes, N. Matlis, K. Nakamura, J. P. O'Neil, B. H. Shaw, S. Steinke, J. van Tilborg, and W. P. Leemans, Measured bremsstrahlung photonuclear production of ^{99}Mo (^{99m}Tc) with 34 MeV to 1.7 GeV electrons, Appl. Radiat. Isot. **96**, 122 (2015).

[30] S. Sekimoto, K. Tatenuma, Y. Suzuki, A. Tsuguchi, A. Tanaka, T. Tadokoro, Y. Kani, Y. Morikawa, A. Yamamoto, and T. Ohtsuki, Separation and purification of ^{99m}Tc from ^{99}Mo produced by electron linear accelerator, J. Radioanal. Nucl. Chem. **311**, 1361 (2017).

[31] B. Szpunar, C. Rangacharyulu, S. Daté, and H. Ejiri, Estimate of production of medical isotopes by photo-neutron reaction at the Canadian Light Source, Nucl. Instrum. Methods Phys. Res., Sect. A **729**, 41 (2013).

[32] R. G. Bennett, J. D. Christian, D. A. Petti, W. K. Terry, and S. B. Grover, A system of ^{99m}Tc production based on distributed electron accelerators and thermal separation, Nuclear Technology **126**, 102 (1999).

[33] K. Gagnon, F. Bénard, M. Kovacs, T. J. Ruth, P. Schaffer, J. S. Wilson, and S. A. McQuarrie, Cyclotron production of ^{99m}Tc: Experimental measurement of the ^{100}Mo$(p,x)^{99}$Mo, ^{99m}Tc and ^{99g}Tc excitation functions from 8 to 18 MeV, Nucl. Med. Biol. **38**, 907 (2011).

[34] O. Lebeda, E. J. van Lier, J. Štursa, J. Ráliš, and A. Zyuzin, Assessment of radionuclidic impurities in cyclotron produced ^{99m}Tc, Nucl. Med. Biol. **39**, 1286 (2012).

[35] S. V. Selivanova, E. Lavallée, H. Senta, L. Caouette, J. A. Sader, E. J. van Lier, A. Zyuzin, J. E. van Lier, B. Guérin, and E. Turcotte, Radioisotopic purity of sodium pertechnetate ^{99m}Tc produced with a medium-energy cyclotron: Implications for internal radiation dose, image quality, and release specifications, J. Nucl. Med. **56**, 1600 (2015).

[36] X. Hou, J. Tanguay, M. Vuckovic, K. Buckley, P. Schaffer, F. Bénard, T. J. Ruth, and A. Celler, Imaging study of using radiopharmaceuticals labeled with cyclotron-produced ^{99m}Tc, Phys. Med. Biol. **61**, 8199 (2016).

[37] S. M. Hanna, Applications of *X*-band technology in medical accelerators, in *Proceedings of the 1999 Particle Accelerator Conference, PAC 1999, New York, 1999*, edited by A. U. Luccio and W. W. MacKay (IEEE, New York, 1999), pp. 2516–2518.

[38] T. P. Wangler, *RF Linear Accelerators*, 2nd ed. (Wiley-VCH, Weinheim, 2008).

[39] H. Braun, L. Rinolfi, S. Weisz, A. Ferrari, R. Tomas, G. Geschonke, W. Wuensch, A. Grudiev, E. Jensen, and R. Corsini, CLIC Study Team Report No. CLIC-Note-764, 2008.

[40] R. Tomás, Overview of the compact linear collider, Phys. Rev. ST Accel. Beams **13**, 014801 (2010).

[41] M. Uesaka, T. Natsui, K. Lee, K. Dobashi, T. Yamamoto, T. Fujiwara, H. Zhu, K. Demachi, E. Tanabe, M. Yamamoto, N. Nakamura, J. Kusano, T. Higo, S. Fukuda, M. Yoshida, and S. Matsumoto, 950 keV, 3.95 MeV and 6 MeV *X*-band linacs for nondestructive evaluation and medicine, Nucl. Instrum. Methods Phys. Res., Sect. A **657**, 82 (2011).

[42] J. Shao, Y. Du, H. Zha, J. Shi, Q. Gao, Q. Jin, H. Chen, W. Huang, C. Tang, J. Xiao, W. Sheng, Y. Han, and C. Wang, Development of a *C*-band 6 MeV standing-wave linear accelerator, Phys. Rev. ST Accel. Beams **16**, 090102 (2013).

[43] E. A. Knapp, B. C. Knapp, and J. M. Potter, Standing wave high energy linear accelerator structures, Rev. Sci. Instrum. **39**, 979 (1968).

[44] D. H. Whittum, Microwave electron linacs for oncology, in *Reviews of Accelerator Science and Technology*, Vol. 2, edited by A. W. Chao and W. Chou (World Scientific, Singapore, 2009), pp. 63–92.

[45] A. J. Koning and D. Rochman, Modern nuclear data evaluation with the TALYS code system, Nucl. Data Sheets **113**, 2841 (2012).

[46] Y. Y. Lau, Classification of Beam Breakup Instabilities in Linear Accelerators, Phys. Rev. Lett. **63**, 1141 (1989).

[47] J. Jang, M. Yamamoto, and M. Uesaka, Development of a compact *X*-band electron linac for production of Mo-99/Tc-99*m*, in *Proceedings of the 7th International Particle Accelerator Conference, IPAC 2016, Busan, Korea, 2016*, edited by K. S. Kim *et al.* (JACoW, Geneva, 2016), pp. 1917–1920.

[48] H. Bateman, The solution of a system of differential equations occurring in the theory of radioactive transformations, Proc. Cambridge Philos. Soc. **15**, 423 (1910).

[49] J. K. Shultis and R. E. Faw, *Fundamentals of Nuclear Science and Engineering*, 2nd ed. (CRC Press, Boca Raton, 2008).

[50] F. B. Brown, Los Alamos National Laboratory Report No. LA-UR-16-29043, 2016.

[51] T. Sato, K. Niita, N. Matsuda, S. Hashimoto, Y. Iwamoto, S. Noda, T. Ogawa, H. Iwase, H. Nakashima, T. Fukahori, K. Okumura, T. Kai, S. Chiba, T. Furuta, and L. Sihver, Particle and Heavy Ion Transport code System, PHITS, version 2.52, J. Nucl. Sci. Technol. **50**, 913 (2013).

[52] H. Hirayama, Y. Namito, A. F. Bielajew, S. J. Wilderman, and W. R. Nelson, SLAC (United States) Report No. SLAC-R-730, and KEK (Japan) Report No. 2005-8, 2005.

[53] S. Hanna, *RF Linear Accelerators for Medical and Industrial Applications* (Artech House, Norwood, 2012).

[54] W. P. Swanson, *Radiological Safety Aspects of the Operation of Electron Linear Accelerators*, IAEA Technical Reports Series Vol. 188 (International Atomic Energy Agency, Vienna, 1979).

[55] R. M. Barnett *et al.*, Review of particle physics, Phys. Rev. D **54**, 1 (1996).

[56] T. Anno, Y. Okubo, and T. Tanaka, Development of the *X*-band 6 MW pulsed klystron (in Japanese), in *Proceedings of the 12th Annual Meeting of Particle Accelerator Society of Japan, PASJ 2015, Tsuruga, Japan, 2015* (PASJ, Tokyo, 2015), pp. 1129–1132.

[57] R. E. Collin, *Foundations for Microwave Engineering*, 2nd ed. (McGraw-Hill, Singapore, 1992), Sec. III.17.

[58] D. M. Pozar, *Microwave Engineering*, 4th ed. (Wiley, Hoboken, 2012), p. 719.

[59] J. H. Billen and L. M. Young, POISSON/SUPERFISH on PC compatibles, in *Proceedings of the 1993 Particle Accelerator Conference, PAC 1993, Washington, DC, 1993*, edited by S. T. Corneliussen and L. Carlton (IEEE, New York, 1993), pp. 790–792.

[60] A. S. Alimov, D. I. Ermakov, B. S. Ishkhanov, E. A. Knapp, V. I. Shvedunov, and W. P. Trower, Industrial high-current electron linacs, in *Proceedings of the 7th European Particle Accelerator Conference, EPAC 2000, Vienna, Austria, 2000*, edited by J. L. Laclare *et al.* (Austrian Academy of Sciences Press, Geneva, 2000), pp. 803–805.

[61] M. Yamamoto, Accuthera Inc. Report No. EM-15098A, 2016 (unpublished).

[62] S. B. van der Geer and M. J. de Loos, GENERAL PARTICLE TRACER: A 3D code for accelerator and beam line design, in *Proceedings of the 5th European Particle Accelerator Conference, EPAC 1996, Barcelona, Spain, 1996*, edited by S. Myers *et al.* (Institute of Physics Publishing, Bristol, 1996), pp. 1245–1247.

[63] Japan Atomic Energy Commission, Action plan for the stable supply of technetium radiopharmaceuticals in Japan (in Japanese), 28th Commissioners' Meeting Material No. 2-1, Japan Atomic Energy Commission, 2011.

[64] OECD Nuclear Energy Agency, *The Supply of Medical Radioisotopes: An Assessment of Long-term Global Demand for Technetium-99m* (OECD, Paris, 2011).

[65] OECD Nuclear Energy Agency, *The Supply of Medical Radioisotopes: 2017 Medical Isotope Supply Review: ^{99}Mo/^{99m}Tc Market Demand and Production Capacity Projection 2017-2022* (OECD, Paris, 2017).

[66] Science Council of Japan, On the stable supply system of radioisotopes in Japan (in Japanese), 60th Executive Board Meeting Material, 2008.

[67] T. Yamashita, in *The OECD-NEA HLG-MR Meeting, Paris, France, 2013*, http://www.jrias.or.jp/e/pdf/Y130710OECD.pdf.

[68] K. Tatenuma, K. Ishikawa, A. Tsuguchi, Y. Komatsuzaki, Y. Suzuki, A. Tanaka, K. Kurosawa, T. Uehara, Y. Higaki, H. Hanaoka, and Y. Arano, A mass-production process of a highly pure medical use ^{99m}Tc from natural isotopic Mo(n, γ) ^{99}Mo without using uranium, Radioisotopes **63**, 501 (2014).

[69] G. E. Dale, S. D. Chemerisov, G. F. Vandegrift, K. A. Woloshun, C. T. Kelsey IV, P. Tkac, V. Makarashvili, C. D. Jonah, E. R. Olivas, M. A. Holloway, K. P. Hurtle, F. P. Romero, D. A. Dalmas, and J. T. Harvey, Design and experimental activities supporting commercial U.S. electron accelerator production of Mo-99, AIP Conf. Proc. **1525**, 355 (2013).

[70] L. Zheng, Master's thesis, University of New Mexico, 2015.

[71] J. J. M. de Goeij and M. L. Bonardi, How do we define the concepts specific activity, radioactive concentration, carrier, carrier-free and no-carrier-added?, J. Radioanal. Nucl. Chem. **263**, 13 (2005).

[72] U. Holzwarth, Radiopharmaceutical production, in *Radiation Physics for Nuclear Medicine*, edited by M. C. Cantone and C. Hoeschen (Springer-Verlag, Berlin, 2011), p. 79.

[73] R. Chakravarty, R. Ram, A. Dash, and M. R. A. Pillai, Preparation of clinical-scale ^{99}Mo/^{99m}Tc column generator using neutron activated low specific activity ^{99}Mo and nanocrystalline γ-Al$_2$O$_3$ as column matrix, Nucl. Med. Biol. **39**, 916 (2012).

[74] P. Tkac, D. A. Rotsch, M. A. Brown, V. Makarashvili, and G. F. Vandegrift, Chemical processing activities for ^{99}Mo production by (γ, n) and (n, γ) reactions using enriched ^{100}Mo and ^{98}Mo targets, in *Proceedings of the 2015 Mo-99 Topical Meeting, Boston, Massachusetts, 2015*, http://mo99.ne.anl.gov/2015/pdfs/papers/S11P4_Paper_Tkac.pdf.

[75] D. B. Pelowitz, Los Alamos National Laboratory Report No. LA-CP-11-00438, 2011.